Oxidation of Metals (2022) 97:599–627
https://doi.org/10.1007/s11085-022-10106-6

ORIGINAL PAPER

# The Oxidation of Four Co-20Ni-xCr-yAl ($x = 8,15$ wt.%; $y = 3,5$ wt.%) Alloys Under 1 atm $O_2$ at 800 °C and 900 °C

**Y. L. Lv[1] · Y. J. Ren[1] · M. N. Zhou[1] · K. K. Feng[1] · J. Chen[1] · Y. Niu[1]**

Received: 10 January 2022 / Revised: 27 February 2022 / Accepted: 2 March 2022 /
Published online: 5 April 2022


## Abstract

The oxidation of four Co-20Ni-xCr-yAl ($x = 8,15$ wt.%; $y = 3,5$ wt.%) alloys under 1 atm $O_2$ for 24 h was studied at 800 and 900 °C. All the alloys formed complex scales, irregular both in thickness and composition. The formation of external alumina scales was more favored at 800 °C than at 900 °C and for larger chromium and aluminum contents, but was never complete. The simultaneous presence of chromium and aluminum is beneficial for increasing the oxidation resistance of these alloys with respect to ternary Co-20Ni-xCr and Co-20Ni-yAl alloys of similar composition. However, an Al content of 5 wt.% is not yet sufficient to form continuous alumina scales even when coupled with 15 wt.% Cr. The partial substitution of cobalt by nickel has a beneficial effect on the ability of the quaternary Co-20Ni-xCr-yAl alloys to form protective external alumina scales in comparison with the ternary Co-Cr-Al alloys with similar chromium and aluminum contents.

**Keywords** Co-Ni-Cr-Al alloys · High temperature oxidation · Nature of scales · Oxide maps

## Introduction

The high temperature oxidation resistance of metallic materials is based on the formation of stable, continuous, slowly-growing and well-adherent scales, such as alumina and chromia [1–5]. In particular, at high temperatures, i.e., above 900–1000 °C and under high oxygen pressures [5, 6] chromia easily reacts with oxygen to produce

✉ Y. J. Ren
yjren@csust.edu.cn

✉ Y. Niu
yniu@csust.edu.cn

[1] School of Energy and Power Engineering, Changsha University of Science and Technology, Changsha, China

the volatile species $CrO_3$, resulting in scales not sufficiently protective. However, a similar process may also occur below 900 °C in the presence of water vapor due to the formation of another volatile compound, the chromium hydroxide $Cr(OH)_2O_2$ [1], so that under some conditions the formation of alumina may be preferable even at relatively low temperatures. The aluminum content needed to form exclusive alumina scales on Al-containing alloys must exceed a critical value, which, in the absence of chromium, is generally so high to have a strong detrimental effect on their mechanical properties. However, a good combination of mechanical properties and oxidation resistance of alumina-former alloys may be obtained by reducing this critical aluminum content by means of the so-called Third Element Effect (TEE) [1, 5]. This involves the presence of an additional component, usually chromium, forming an oxide with a thermodynamic stability intermediate between those of aluminum and of the base metals which allows to avoid the internal oxidation of aluminum by lowering the oxygen pressure prevailing at the alloy/scale interface. The high-temperature oxidation behavior of ternary Co-Cr-Al and Ni-Cr-Al alloys, representing common examples of the application of TEE and forming the basis of many superalloys [1], has been intensively investigated so far [7–18].

The effects of the simultaneous presence of cobalt and nickel and of the Co/Ni ratio on the high temperature oxidation of Co–Ni-based alloys containing aluminum and chromium have been examined many times for various multi-component materials [19–30]. Weiser et al. [24, 29] reported that the gradual replacement of cobalt by nickel in Co-Ni-Cr-Al-W alloys produced a decrease in their oxidation rates in air at 900 °C. Gao et al. [21] and Zenk et al. [30] showed that the addition of nickel to complex $\gamma/\gamma'$-strengthened cobalt-based superalloys had a positive effect on their oxidation in air at 900 °C. Ismail et al. [23] reported that increasing the cobalt content had an adverse effect on the oxidation of Co-Ni-Cr-Al-W-Ta alloys in air at 800 °C. In general, it as observed that the increase the nickel content in Co-Ni alloys is beneficial for their oxidation behavior, a result which may be related to the differences between the free energies of formation [1] and the growth rates of the nickel and cobalt oxides as well as to differences in the solubility and diffusivity of oxygen in the two base metals [1, 31]. More specifically, the oxidation in air at 900 °C and 950 °C of a number of quaternary Co-Ni-Cr-Al alloys deposited as coatings on an inert substrate by magnetron sputtering was studied by Seraffon et al. [25, 26]. In spite of some limitations, such as the reduced thickness of the samples and an uneven composition of the materials examined caused by the preparation method adopted, these studies still provided a general background concerning the behavior of this type of alloys, allowing to draw approximate oxide maps showing the area of stability of the external alumina scales in pseudo-ternary phase diagrams of the M-Cr-Al type (with $M$ = Co,Ni). Some studies have also been carried out to improve the high temperature oxidation performance of Co-Ni-Cr-Al alloys by the addition of active elements [27, 28].

In spite of the previous work, the high-temperature oxidation behavior of Co-Ni-Cr-Al alloys has not been completely elucidated so far, particularly for what concerns the effects of changes of the Co/Ni ratio on the high temperature oxidation performance of bulk Co-Ni-Cr-Al alloys, so that further research is still needed. The present paper examines the isothermal oxidation behavior of four Co-20Ni-xCr-yAl

($x = 8,15$ wt.%; $y = 3,5$ wt.%) alloys exposed to 1 atm $O_2$ at 800 °C and 900 °C for 24 h, exploring the effects of the different chromium and aluminum contents on their oxidation resistance and on the microstructure of the scales produced. The scaling behavior of these four alloys exposed to the same environment at 1000 °C and 1100 °C has already been discussed in a previous paper [32].

## Experimental Procedures

The four alloys with nominal composition (wt.%, if not specified otherwise) Co-20Ni-xCr-yAl ($x = 8$, 15; $y = 3$, 5) used in the experiment were made by vacuum induction melting appropriate amounts of high purity metals (Co: 99.9%, Ni: 99.9%, Cr: 99%, Al: 99.7%) and then cast into cylinders 10 cm high and with a diameter of 5 cm. Subsequently, the alloy ingots were annealed in 1 atm argon at 1000 °C for 36 h to release the residual stresses and to achieve a good homogenization. Their actual composition, measured by ICP spectroscopy, is shown in Table 1. According to the micrographs of the four alloys reported in a previous paper [32], three alloys (Co-20Ni-8Cr-3Al, Co-20Ni-8Cr-5Al and Co-20Ni-15Cr-3Al) are single-phase even at room temperature, while Co-20Ni-15Cr-5Al is made of a Co-Ni matrix with a small content of a second phase rich in nickel and internal oxidation zone. Finally, the grain sizes of the four alloys are large enough to exclude any special effect of this factor on their corrosion behavior.

The ingots were cut into samples with an approximate size of $10 \times 8 \times 1.5$ mm using a line saw, drilling a circular hole with a diameter of about 1 mm near one edge. Each sample was metallographically polished down to 2000 grit finish according to EU standard and then ultrasonically cleaned in acetone and ethanol immediately before exposure. The corrosion tests were carried out in 1 atm of pure oxygen with a flow rate of 100 ml/min at 800 °C and 900 °C, measuring the mass changes using a microbalance (Setaram B-92). At the beginning of each test the sample was suspended with Pt wire in the balance under a flux of argon of 100 ml/min, while the furnace was heated up separately with a heating rate of 30 K/min. After reaching the test temperature the furnace was raised to the sample level ad oxygen was introduced into the reaction chamber. The duration of all tests was of 24 h. At the end of each test the samples were allowed to cool down to room temperature inside the furnace in an argon atmosphere.

**Table 1** Nominal and actual composition of the four Co-20Ni-xCr-yAl ($x = 8,15$ wt.%; $y = 3,5$ wt.%) alloys measured by ICP spectrometry analysis

| Nominal (wt.%) | Nominal (at.%) | Actual (ICP wt.%) |
|---|---|---|
| Co-20Ni-8Cr-3Al | Co-19.27Ni-8.65Cr-6.23Al | Co-20.1Ni-7.99Cr-3.02Al |
| Co-20Ni-8Cr-5Al | Co-18.94Ni-8.38Cr-10.26Al | Co-20.2Ni-7.92Cr-5.03Al |
| Co-20Ni-15Cr-3Al | Co-19.02Ni-15.96Cr-6.14Al | Co-20.0Ni-14.87Cr-2.97Al |
| Co-20Ni-15Cr-5Al | Co-18.23Ni-15.53Cr-10.12Al | Co-19.6Ni-14.79Cr-5.00Al |

**Fig. 1** Kinetic curves for the oxidation of Co-20Ni-xCr-yAl ($x = 8{,}15$ wt.%; $y = 3{,}5$ wt.%) alloys in 1 atm ▶ $O_2$ at 800 °C for 24 h: **a** Linear plots; **b** Parabolic plots; **c** Enlarged view of the parabolic plots for the alloys Co-20Ni-15Cr-yAl

The corroded samples were examined by scanning electron microscopy (SEM, FEI INSPECTF 50, USA), energy dispersive spectrometer (EDS, OXFORD X-MAX, UK), X-ray diffraction (XRD, Panalytical X' pert PRO, Holland) and electron probe microanalysis (EPMA, EPMA-1610) to identify the element distribution and the morphology and phase constitution of the scales.

## Results

### Corrosion Kinetics

The kinetic curves for the oxidation of the four alloys in 1 atm $O_2$ at 800 °C for 24 h are shown in Fig. 1a as linear plots and in Fig. 1b, c as parabolic plots, respectively. For Co-20Ni-8Cr-3Al oxidized at 800 °C, an initial stage of about 30 min with an instantaneous parabolic rate parameter (iprp, i.e., the instantaneous slope of the parabolic plot) increasing with time was followed by a parabolic stage lasting until the end of the test with a parabolic rate constant $k_p = 2.12 \times 10^{-11}$ $g^2cm^{-4}$ $s^{-1}$. For Co-20Ni-8Cr-5Al an initial stage of about 30 min was followed by two stages. The first stage, lasting from 30 min to 16 h, was parabolic with $k_p = 2.09 \times 10^{-11}$ $g^2cm^{-4}$ $s^{-1}$, while the second stage had an iprp decreasing slightly with time with a final $k_p = 1.50 \times 10^{-11}$ $g^2cm^{-4}$ $s^{-1}$. The corrosion of Co-20Ni-15Cr-3Al also included two stages: an initial parabolic stage, lasting 2.5 h with $k_p = 1.45 \times 10^{-12}$ $g^2cm^{-4}$ $s^{-1}$, was followed by a second quasi-parabolic stage, lasting up to the end of the test, with an iprp gradually initially decreasing and finally increasing with time with an average $k_p$ value of $2.84 \times 10^{-13}$ $g^2cm^{-4}$ $s^{-1}$. A similar behavior was also followed by Co-20Ni-15Cr-5Al, with an initial parabolic stage lasting from 30 min to 2 h with $k_p = 3.71 \times 10^{-12}$ $g^2cm^{-4}$ $s^{-1}$ and a second quasi-parabolic stage with $k_p = 1.21 \times 10^{-13}$ $g^2cm^{-4}$ $s^{-1}$.

The kinetic curves for the oxidation of the four alloys in 1 atm $O_2$ at 900 °C for 24 h are shown in Fig. 2a as linear plots and in Fig. 2b, c as parabolic plots, respectively. Co-20Ni-8Cr-3Al behaved similarly to 800 °C, showing an initial stage of about 30 min followed by a parabolic stage with a rate constant $k_p = 1.89 \times 10^{-9}$ $g^2cm^{-4}$ $s^{-1}$. Co-20Ni-8Cr-5Al had an initial parabolic stage lasting approximately from 15 min to 9 h with a rate constant $k_p = 8.71 \times 10^{-10}$ $g^2cm^{-4}$ $s^{-1}$ followed by the second stage with an iprp gradually decreasing with time down to a final value of $4.58 \times 10^{-10}$ $g^2cm^{-4}$ $s^{-1}$. Co-20Ni-15Cr-3Al had a similar behavior, with an initial parabolic stage, from 40 min to 7 h with $k_p = 7.68 \times 10^{-11}$ $g^2cm^{-4}$ $s^{-1}$ followed by the second stage with an iprp gradually decreasing with time with an average $k_p$ value of $1.84 \times 10^{-11}$ $g^2cm^{-4}$ $s^{-1}$. After an initial stage of very low rate up to 1 h, Co-20Ni-15Cr-5Al followed by two approximately parabolic stages: the first stage, lasting

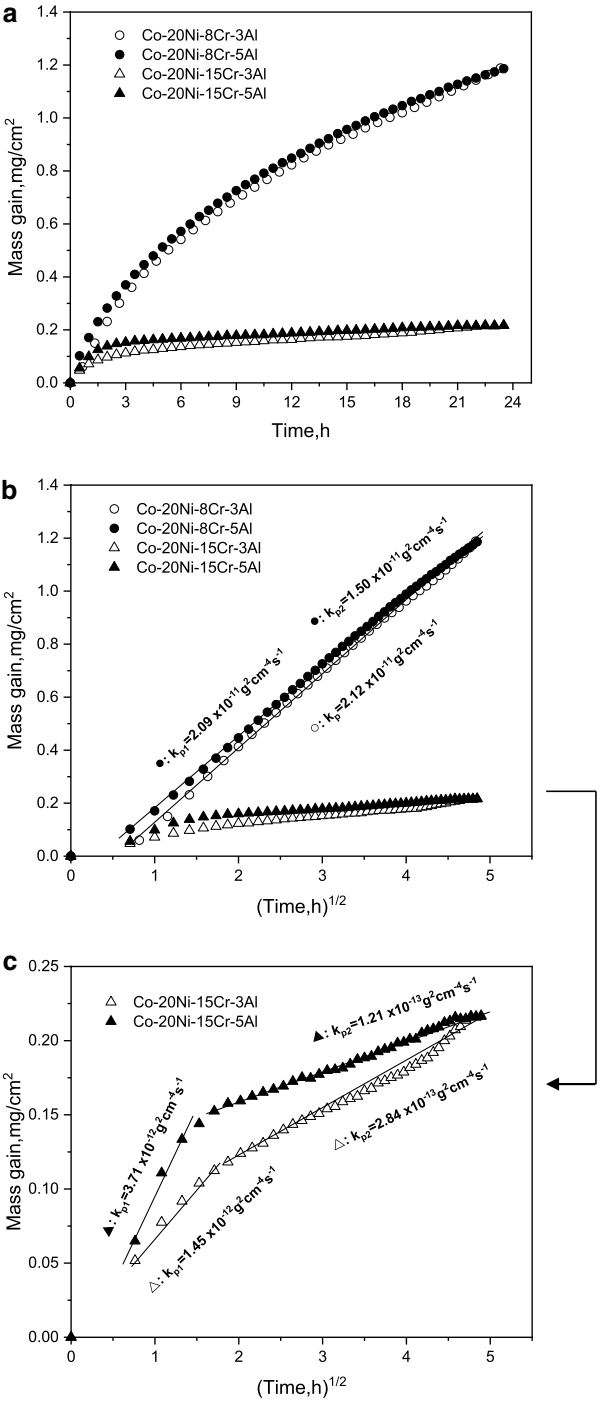
a
Co-20Ni-8Cr-3Al
Co-20Ni-8Cr-5Al
Co-20Ni-15Cr-3Al
Co-20Ni-15Cr-5Al
Mass gain,mg/cm2
Time,h
b
Co-20Ni-8Cr-3Al
Co-20Ni-8Cr-5Al
Co-20Ni-15Cr-3Al
Co-20Ni-15Cr-5Al
●: kp1=2.09 x10-11 g2cm-4s-1
●: kp2=1.50 x10-11 g2cm-4s-1
○: kp2=2.12 x10-11 g2cm-4s-1
Mass gain,mg/cm2
(Time,h)1/2
c
Co-20Ni-15Cr-3Al
Co-20Ni-15Cr-5Al
▲: kp1=3.71 x10-12 g2cm-4s-1
▲: kp2=1.21 x10-13 g2cm-4s-1
△: kp1=1.45 x10-12 g2cm-4s-1
△: kp2=2.84 x10-13 g2cm-4s-1
Mass gain,mg/cm2
(Time,h)1/2

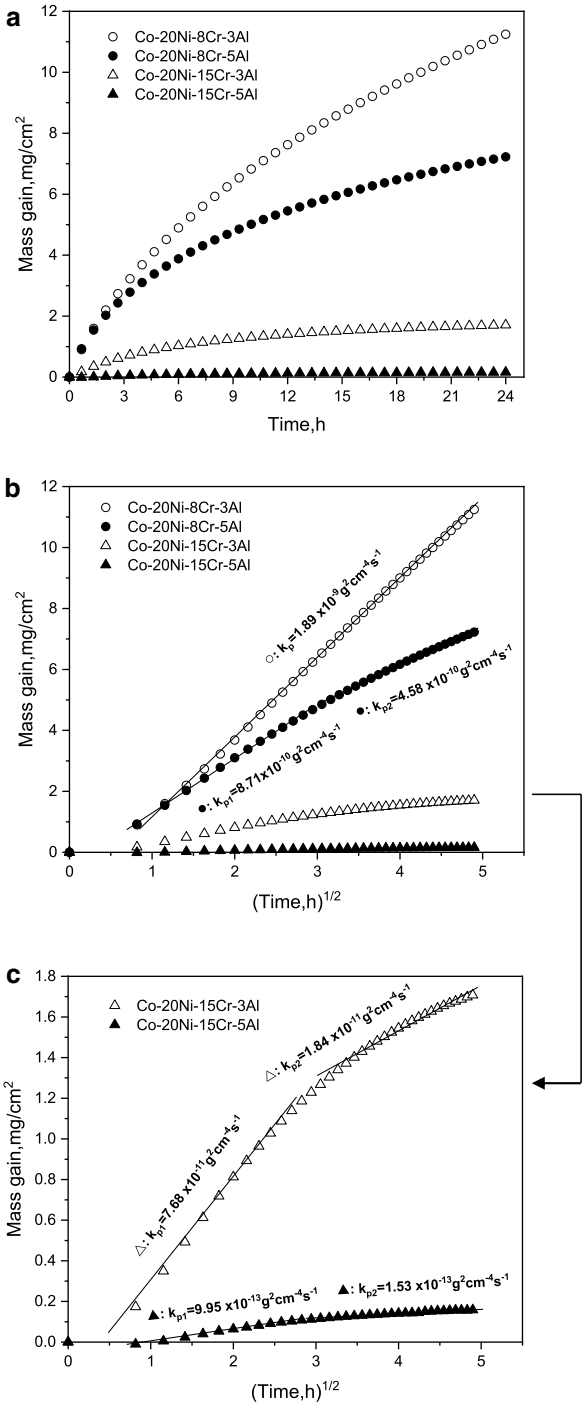


**Fig. 2** Kinetic curves for the oxidation of Co-20Ni-xCr-yAl ($x$=8,15 wt.%; $y$=3,5 wt.%) alloys in 1 atm $O_2$ at 900 °C for 24 h: **a** Linear plots; **b** Parabolic plots; **c** Enlarged view of the parabolic plots for the alloys Co-20Ni-15Cr-yAl

from 1 to 9 h with $k_p = 9.95 \times 10^{-13}$ $g^2cm^{-4}$ $s^{-1}$, was followed by a second stage, lasting from 9 h to the end of the test, with $k_p = 1.53 \times 10^{-13}$ $g^2cm^{-4}$ $s^{-1}$.

In summary, at 800 °C the two alloys with 8 wt.% Cr corroded at similar rates, but much faster than the two alloys with 15 wt.% Cr, which again behaved similarly. Conversely, at 900 °C the oxidation rates of the four alloys were significantly different and decreased in the order Co-20Ni-8Cr-3Al > Co-20Ni-8Cr-5Al > Co-20Ni-15Cr-3Al > Co-20Ni-15Cr-5Al. These results suggest that at 800 °C the oxidation rates are essentially controlled by the chromium content, while the increase of the aluminum content from 3 to 5 wt.% has only a small effect. Conversely, at 900 °C the increase of the aluminum content from 3 to 5 wt.% under a constant chromium content has a beneficial effect on the corrosion resistance for both the alloys containing either 8 wt.% or 15 wt.% chromium.

Figure 3 shows again separately the linear plots of the kinetic curves for each of the four alloys at 800 °C and 900 °C, including also the corresponding results obtained previously for the oxidation of the same alloys for 20 h at 1000 °C and 1100 °C, published recently [32], to show more clearly the effect of temperature on their corrosion behavior. The mass gains of Co-20Ni-8Cr-3Al (Fig. 3a) increase

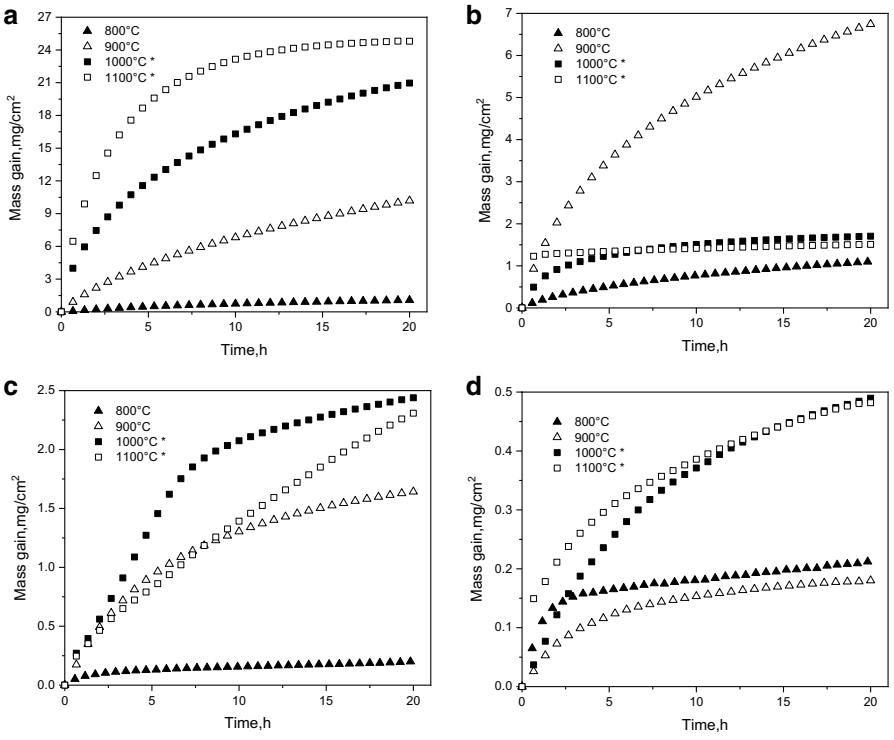


**Fig. 3** Temperature effect on the kinetic curves for the oxidation of the Co-20Ni-xCr-yAl ($x = 8$, 15 wt.%; $y = 3$, 5 wt.%) alloys in 1 atm $O_2$ at 800 °C, 900 °C, 1000 °C (*) and 1100 °C (*) for 20 h: **a** Co-20Ni-8Cr-3Al; **b** Co-20Ni-8Cr-5Al; **c** Co-20Ni-15Cr-3Al; **d** Co-20Ni-15Cr-5Al. (*)—data from Ref [32]

regularly with temperature, but the final slope of the curve at 1100 °C is significantly lower than that at 1000 °C, so the two curves might cross each other over a longer period of time. For Co-20Ni-8Cr-5Al the mass gains at 900 °C are far greater than at the other three temperatures, while those measured at 800 °C are the smallest: moreover, and the values measured at 1000 °C and 1100 °C are comparable even though the final slope of the curve at 1100 °C is smaller than that observed at 1000 °C. The mass gains of Co-20Ni-15Cr-3Al increase with temperature, especially in going from 800 to 900 °C. The mass gains at 1100 °C are smaller than those measured at 1000 °C, but the final slope of the curve at 1100 °C is significantly higher than that at 1000 °C, so that even in this case the two curves may cross each other at longer times. For Co-20Ni-15Cr-5Al the mass gains measured at 800 °C are slightly larger than those measured at 900 °C, while the mass gains at 1000 °C and 1100 °C are significantly larger than those measured at the two lower temperatures and cross each other at the end of the test.

In summary, the increase of temperature from 800 to 900 °C has a positive effect on the oxidation resistance of Co-20Ni-15Cr-5Al, while it has a negative effect on the other three alloys, resulting in greatly accelerated oxidation rates. Conversely, the increase of temperature from 1000 to 1100 °C has a positive effect for the oxidation of the two alloys with 8 wt.% Cr, but especially for the alloy with 5 wt.% Al, while it has a negative effect for Co-20Ni-15Cr-3Al and nearly no effect for Co-20Ni-15Cr-5Al.

The kinetic curves for the oxidation of the four quaternary alloys for 24 h in 1 atm $O_2$ at 800 °C and 900 °C are compared with those measured for the oxidation for 24 h of the corresponding ternary Co-20Ni-R alloys (with $R$ = Cr or Al) containing only aluminum (either 3 or 5 wt.%) or only chromium (either 8 or 15 wt.%) as well as with those of the binary Co-20Ni alloy in Figs. 4 and 5, respectively. The study of the oxidation of these ternary alloys is presently under way [33], and the relevant data, not yet published, are quoted here only for comparison purposes. An analysis of the data presented in these two figures is postponed to a later section.

## Morphology and Structure of the Scales

Before proceeding to a detailed analysis of the nature of the scales for the various combinations of alloys compositions and temperatures the following general considerations seem appropriate. Due to their insufficient contents of the two reactive components, these alloys are not able to develop continuous external scales made of a slowly-growing oxide, i.e., either chromia or alumina or their combination, which may be able to prevent the oxidation of the two base metals. As a consequence, these alloys generally form scales not uniform in both thickness and composition over different regions of the surface of the same sample. Thus, thin scales made of protective oxides alternate with much thicker scales, frequently grown in the form of oxide nodules, containing also the oxides of the base metal components. In particular, the thick scales are generally composed of two main regions, with external regions made of cobalt and nickel oxides and practically free from both chromium and aluminum associated with internal regions of complex composition, composed of mixtures of

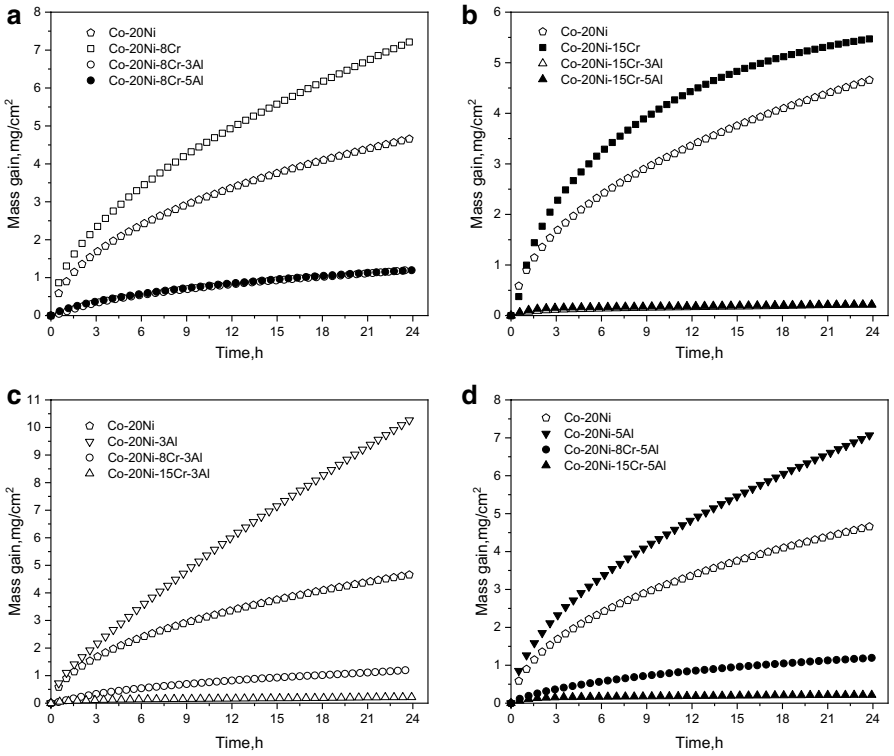


**Fig. 4** Comparison of the kinetic curves for the oxidation in 1 atm $O_2$ at 800 °C for 24 h of the quaternary Co-20Ni-xCr-yAl ($x = 8,15$ wt.%, $y = 3,5$ wt.%) alloys with the corresponding data for the ternary Co-20Ni-xCr and Co-20Ni-yAl alloys and the binary Co-20Ni alloy [33]: **a** Co-20Ni-(0,8)Cr-(0,y)Al; **b** Co-20Ni-(0,15)Cr-(0,y)Al; **c** Co-20Ni-(0,x)Cr-(0,3)Al; **d** Co-20Ni-(0,x)Cr-(0,5) Al

various oxides whose relative importance depends on the overall content of chromium and aluminum of each specific alloy. Thus, alloys with small chromium and aluminum contents form internal regions mostly composed of a solid solution of CoO and NiO, denoted simply as MO in the following, mixed with double oxides of general formula $MR_2O_4$ (where $M = $ Co,Ni and $R = $ Cr,Al), simply denoted hereafter as spinels. Conversely, for alloys richer in chromium and aluminum the mixtures of MO and spinels typical of this region are increasingly replaced by mixtures of the two protective oxides, sometimes indicated collectively as $R_2O_3$. Furthermore, the growth of thick scales is generally associated with the presence of a zone of internal oxidation of aluminum, not observed in the presence of thin scales. Finally, the structure of the external layer of the thick scales differs depending on the reaction temperature. In particular, for samples oxidized at 800 °C this scale layer is composed of an external zone made of the higher cobalt oxide, $Co_3O_4$, practically free from nickel (darker), while the internal zone (lighter) is made by MO. Conversely, for samples oxidized at 900 °C the external region is made almost completely by MO, while $Co_3O_4$ is only present in the form of islands distributed in the outer

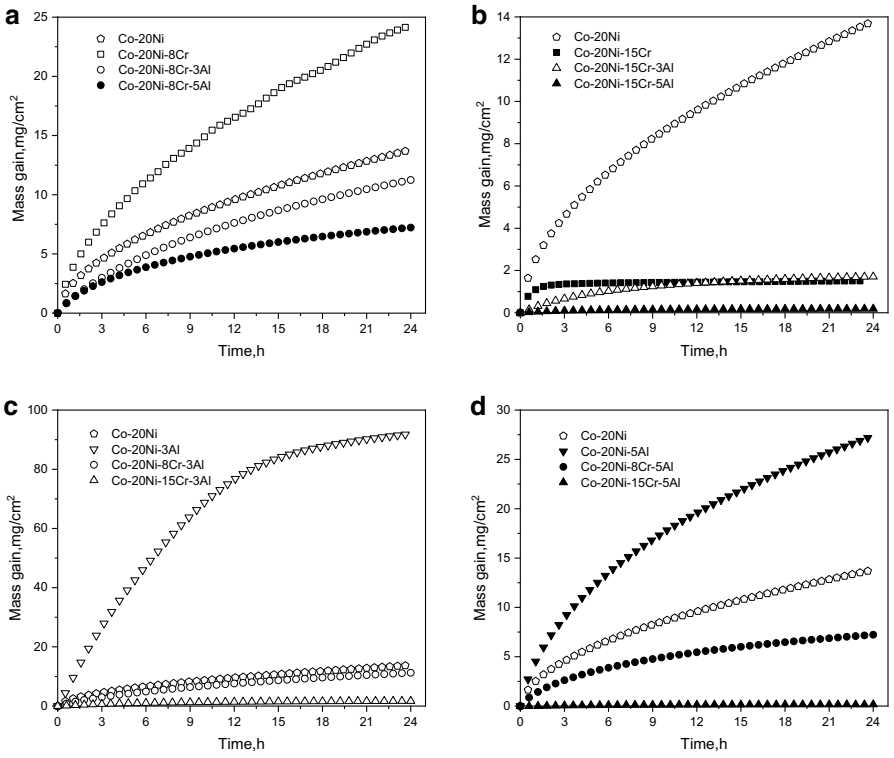


**Fig. 5** Comparison of the kinetic curves for the oxidation in 1 atm $O_2$ at 900 °C for 24 h of the quaternary Co-20Ni-xCr-yAl ($x$ = 8,15 wt.%, $y$ = 3,5 wt.%) alloys with the corresponding data for the ternary Co-20Ni-xCr and Co-20Ni-yAl alloys and the binary Co-20Ni alloy [33]: **a** Co-20Ni-(0,8)Cr-(0,y)Al; **b** Co-20Ni-(0,15)Cr-(0,y)Al; **c** Co-20Ni-(0,x)Cr-(0,3)Al; **d** Co-20Ni-(0,x)Cr-(0,5) Al

fraction of the MO matrix. The reasons for this difference are briefly considered in "Oxidation kinetics" section.

Cross sections of Co-20Ni-8Cr-3Al oxidized at 800 °C are shown in Fig. 6. Most of the alloy surface is covered by a complex scale including a duplex external layer containing an outer zone made of $Co_3O_4$ (darker) and an inner zone (lighter) made of a solid solution of CoO and NiO (MO, lighter), followed by a complex inner layer of irregular thickness located into the alloy consumption zone and containing mixtures of MO with cobalt- nickel- chromium-aluminum spinels. An internal oxidation zone (IOZ) of aluminum is present only at some locations beneath the thick scale layer (Fig. 6b). A small fraction of the alloy surface is covered by a thin alumina scale and is free from internal oxidation (Fig. 6a, c). Finally, the scale contains also nodules (Fig. 6c) presenting a structure similar to that of the continuous scale shown in Fig. 6b and overlying an IOZ of aluminum. The X-ray maps of the nodule in Fig. 6d (Fig. 6e) show that its external section, protruding out of the original alloy surface, is made mostly of Ni-free $Co_3O_4$ with a limited presence of MO in the inner region and does

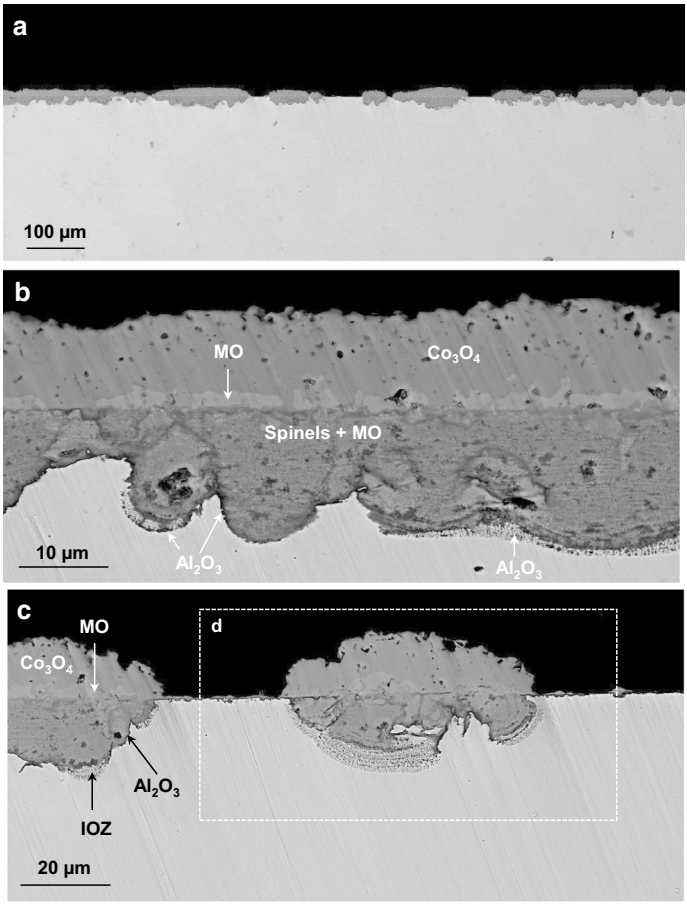


**Fig. 6** Micrographs (SEM/BEI) of cross sections of Co-20Ni-8Cr-3Al oxidized in 1 atm $O_2$ at 800 °C for 24 h: **a** General view; **b** Enlarged view of a thick scale region; **c** Enlarged view of nodules; **d** Enlarged view of the selected area of (**c**); **e** EDS maps of (**d**)

not contain either chromium or aluminum. Conversely, the internal section of the nodule, lying inside the alloy consumption zone, contains all the alloy components, not evenly distributed, indicating the coexistence of different phases. These include MO and spinels, but also some chromia (darker areas), while alumina (black areas) is present mostly as internal oxide particles, but also as a continuous layer at a few locations. Some large metal particles containing nickel and cobalt (white) are also incorporated in the inner scale region.

After oxidation at 900 °C (Fig. 7), the sample of Co-20Ni-8Cr-3Al is covered again by an external scale similar to that observed after oxidation at 800 °C, but thicker and more regular (Fig. 7a). However, the external layer grown at this temperature is mostly composed of MO and contains only some isolated particles of $Co_3O_4$, darker than MO, located in the external region of this layer (Fig. 7b). The

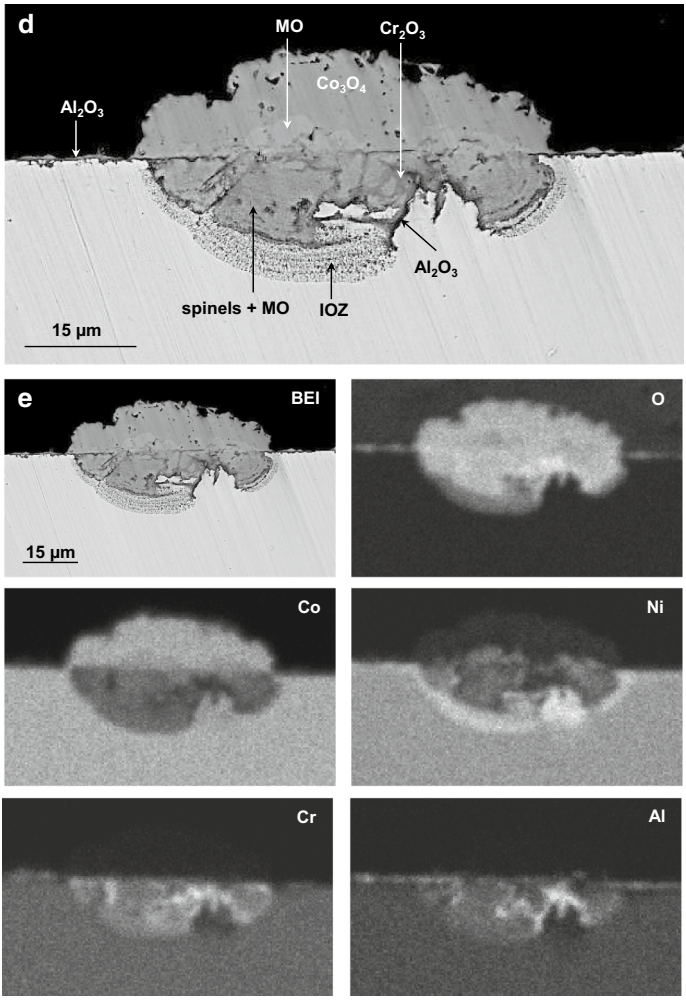


**Fig. 6** (continued)

inner scale region is composed again of MO plus spinels with some streaks of chromia (darker). An IOZ of aluminum is also generally present beneath the alloy/scale interface (Fig. 7a, d), while in few areas a thin continuous layer of alumina has grown in contact with the alloy, preventing the internal precipitation of alumina (Fig. 7b, c).

A cross section of Co-20Ni-8Cr-5Al oxidized at 800 °C for 24 h is shown in Fig. 8. A duplex layer, often in the form of isolated nodules, similar to that described above, formed on less than half of the alloy surface (Fig. 8a, b), sometimes associated with an internal oxidation of aluminum. The remaining fraction of the sample surface is covered by a continuous alumina layer (Fig. 8b). The scale grown on the same alloy after oxidation at 900 °C for 24 h (Fig. 9) is very similar to that observed

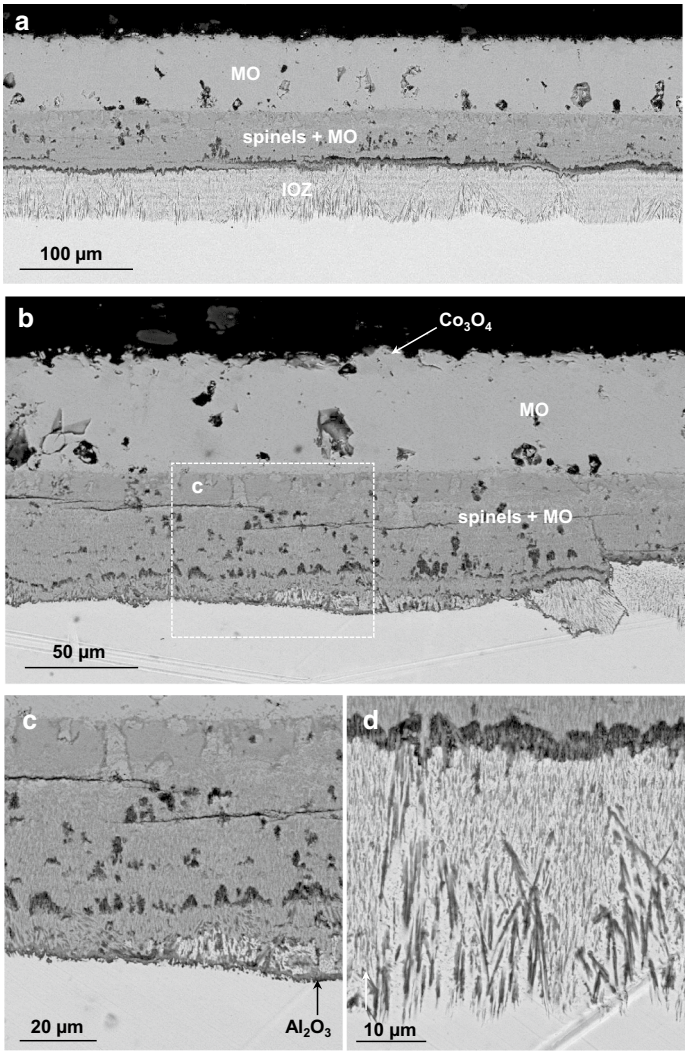


**Fig. 7** Micrographs (SEM/BEI) of cross sections of Co-20Ni-8Cr-3Al oxidized in 1 atm $O_2$ at 900 °C for 24 h: **a** General view; **b** View of a different scale region; **c** Enlarged view of selected area of (**b**); **d** Enlarged view of the internal oxidation zone

on Co-20Ni-8Cr-3Al after oxidation at the same temperature, except for the reduced thickness of the external scale (approximately 40% smaller). Moreover, the thickness of the inner layer is quite irregular and contains regions presenting an IOZ of aluminum alternating with others free from internal oxidation due to the growth of a thin alumina layer in contact with the alloy (Fig. 9a, b). This is shown more clearly by the X-ray maps (Fig. 9c) which indicate again the substantial absence of chromium and aluminum from the external scale region and the preferential concentration of nickel in the inner region of the external scale layer. Moreover, the scale

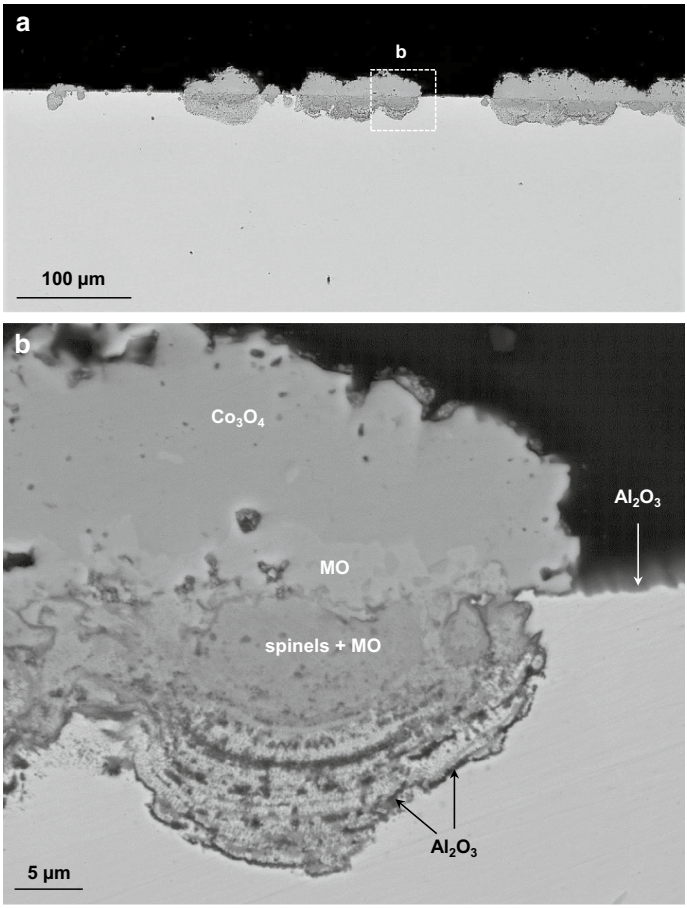


**Fig. 8** Micrographs (SEM/BEI) of a cross section of Co-20Ni-8Cr-5Al oxidized in 1 atm $O_2$ at 800 °C for 24 h: **a** General view; **b** Enlarged view of the selected area of (**a**)

located in the alloy-consumption region contains much more nickel than cobalt and has large contents of both chromium and aluminum. In particular, alumina is either present as a thin but continuous layer (left side of Fig. 9c), or as internal oxide (right side of the same figure). Finally, nickel is strongly enriched in the alloy located inside IOZ and especially around the interface between this zone and the bulk alloy.

Oxidation of 20Ni-15Cr-3Al at 800 °C for 24 h (Fig. 10) formed protective alumina scales on most of the alloy surface (about 80%), while the remaining fraction was covered by a much thicker scale, sometimes in the form of nodules (Fig. 10b, c), presenting the usual duplex structure in the region protruding from the alloy, composed of an outer layer of $Co_3O_4$ (darker) and an inner layer of Ni-rich MO. Conversely, the scale developed in the alloy consumption zone has a complex composition, as shown more clearly by the corresponding X-ray maps (Fig. 10c). The external zone of this region (lighter) is made of a

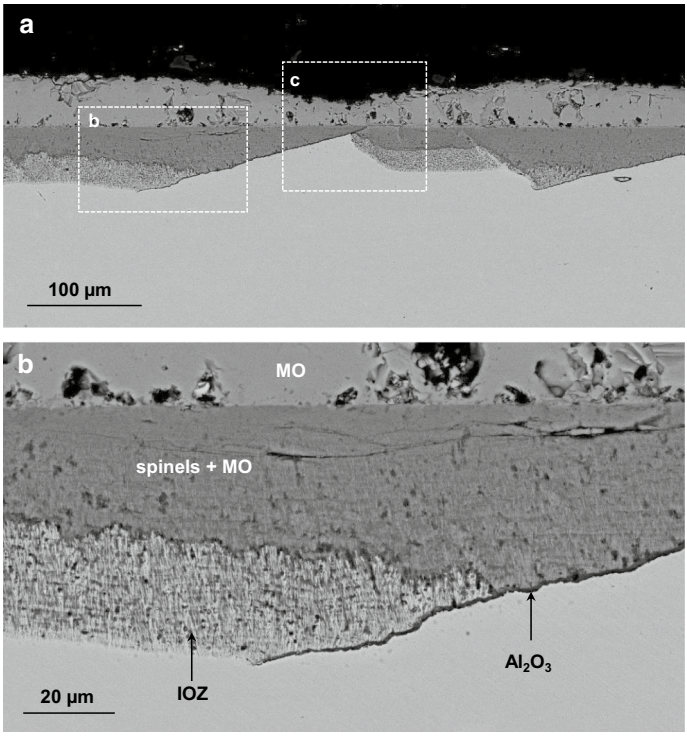


**Fig. 9** Micrographs (SEM/BEI) of a cross section of Co-20Ni-8Cr-5Al oxidized in 1 atm $O_2$ at 900 °C for 24 h: **a** General view; **b** Enlarged view of the selected area of (**a**). **c** Enlarged view and EDS maps of the selected area of (**a**)

mixture of spinels with some MO, while the internal zone is made of a mixture of some Ni-rich spinels with chromium oxide and some aluminum oxide ($R_2O_3$) plus a number of alloy particles (light). The thin boundary between these two zones (darker) is particularly rich in aluminum. Finally, the surface layer of the alloy beneath the nodule contains many isolated alumina particles which at some places form a continuous layer. After oxidation of Co-20Ni-15Cr-3Al at 900 °C for 24 h (Fig. 11) about one half of the sample surface is covered by a duplex scale of uneven thickness (Fig. 11a, b) composed of an external zone of MO with $Co_3O_4$ islands plus an inner zone of MO and spinels with some chromia (darker) overlying a thin irregular region containing small alumina particles (black) tending to form a continuous layer (Fig. 11b). The remaining fraction of the alloy surface is covered by a thin scale (Fig. 11c, d) alternating with some large nodules presenting a structure similar to that of the thick scale regions. Conversely, the thin scales (Fig. 11c, d) are mostly made of chromium oxide incorporating some alloy particles (white) and are followed by alumina particles protruding into the alloy and tending to form a thin even though discontinuous layer.

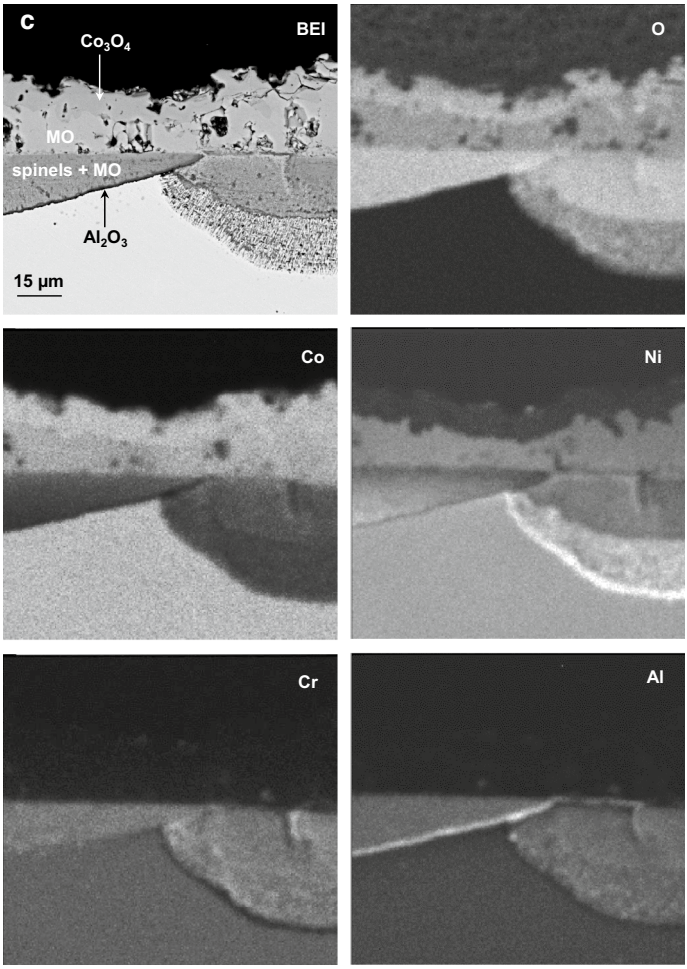


**Fig. 9** (continued)

After 24 h oxidation at 800 °C Co-20Ni-15Cr-5Al formed a very thin alumina layer (Fig. 12) over the largest fraction (about 85%) of the sample surface, while the remainder was covered by nodules (Fig. 12b, c) presenting the usual duplex structure involving an external region made of $Co_3O_4$ with some MO islands plus an internal region containing some spinel islands (Fig. 12c, light), mostly located close to the interface with the external scale layer, but composed mostly of mixtures of aluminum and chromium oxides ($R_2O_3$). Below the nodules alumina tends again to form a nearly continuous layer in contact with the alloy. Oxidation of the same alloy at 900 °C for 24 h formed again irregular scales (Fig. 13). In particular, a small fraction of the alloy surface (about 10%) formed a very thin layer of alumina in contact with the alloy surmounted by a lighter chromia-rich

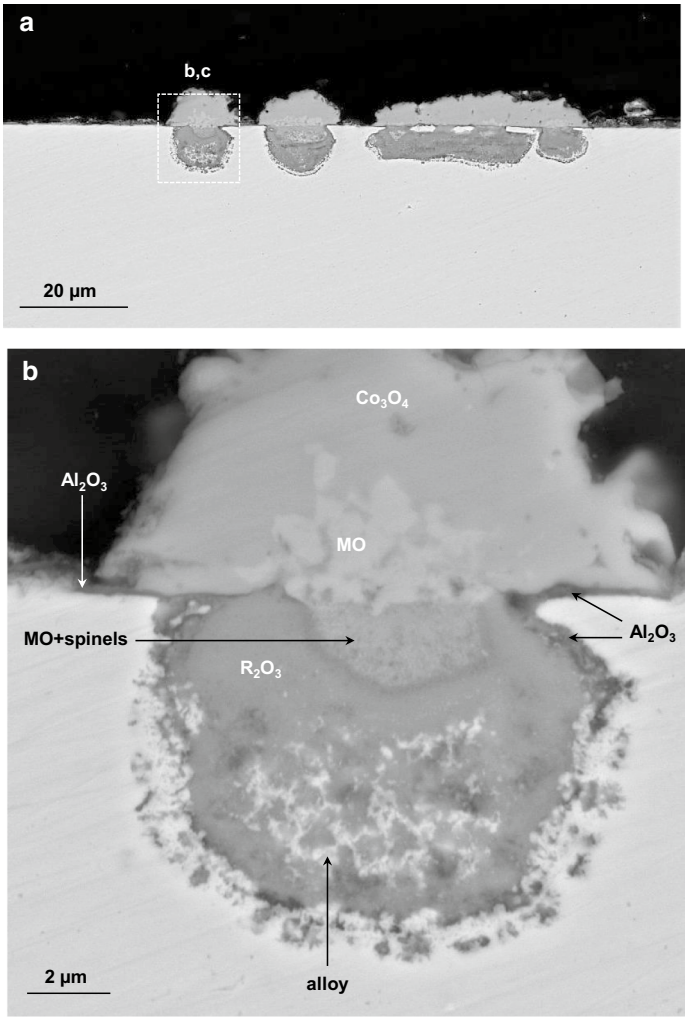


**Fig. 10** Micrographs (SEM/BEI) of a cross section of Co-20Ni-15Cr-3Al oxidized in 1 atm $O_2$ at 800 °C for 24 h: **a** General view; **b** Enlarged view of the selected area of (**a**); **c** EDS maps of (**b**)

layer (central region of Fig. 13a and b). The remainder of the surface formed two types of scale, with approximately the same abundance. In one case (Fig. 13d) the scale, slightly thicker and more complex than that shown in Fig. 13b, includes an external region composed of MO with some $Co_3O_4$ particles followed by an inner darker region. According to the corresponding X-ray maps (Fig. 13e) this region is essentially free from both cobalt and nickel and contains a layer of alumina in contact with the alloy surmounted by a layer of chromia mixed with alumina (darker areas). In view of its composition and of the absence of internal oxidation of aluminum this kind of scale may be considered as substantially equivalent to

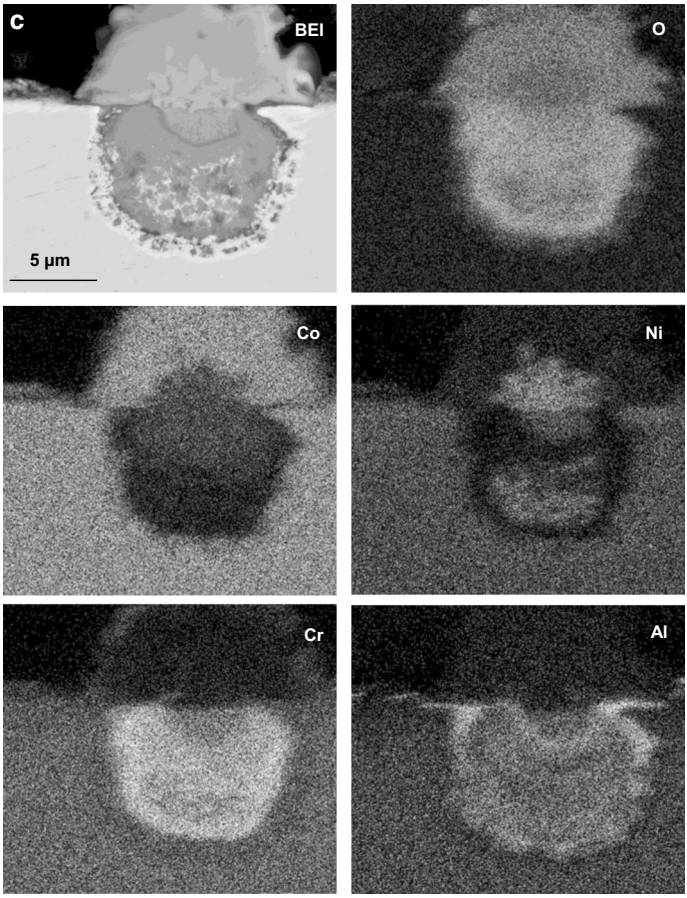


**Fig. 10** (continued)

that shown in Fig. 13b. At other places (Fig. 13c) the scale consists of an external layer composed of an outer region of MO mixed with $Co_3O_4$ plus an inner region made of a mixture of spinels and chromia which contains also many alloy particles (white), sometimes forming a nearly continuous layer. The alloy layer underlying this type of scale contains also a significant volume fraction of large but isolated internal alumina particles.

## Discussion

### Classification of Scales

The nature of the scales formed by the present alloys is first examined by extending, with appropriate modifications, the classification into four types of scales,

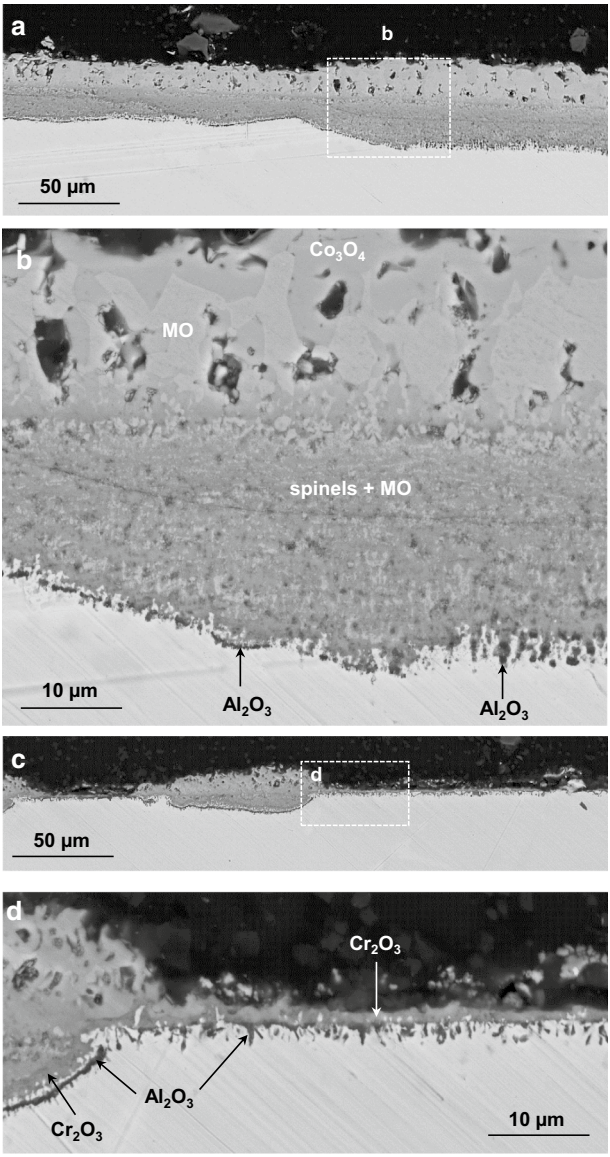


**Fig. 11** Micrographs (SEM/BEI) of cross sections of Co-20Ni-15Cr-3Al oxidized in 1 atm $O_2$ at 900 °C for 24 h: **a** General view of a thick scale region; **b** Enlarged view of the selected area of (**a**); **c** General view of a thin scale region; **d** Enlarged view of the selected area of (**c**)

corresponding to four groups of alloys, proposed for the oxidation of ternary of Co-Cr-Al alloys by Wallwork and Hed [7], to the present case of quaternary Co-20Ni-xCr-yAl alloys. In the case of the ternary Co-Cr-Al system alloys of group I form scales containing an outer thick columnar dense CoO layer and a much thinner inner porous layer made of CoO mixed with $Al_2O_3$, $Cr_2O_3$ and $Co(Cr,Al)_2O_4$ spinels (type

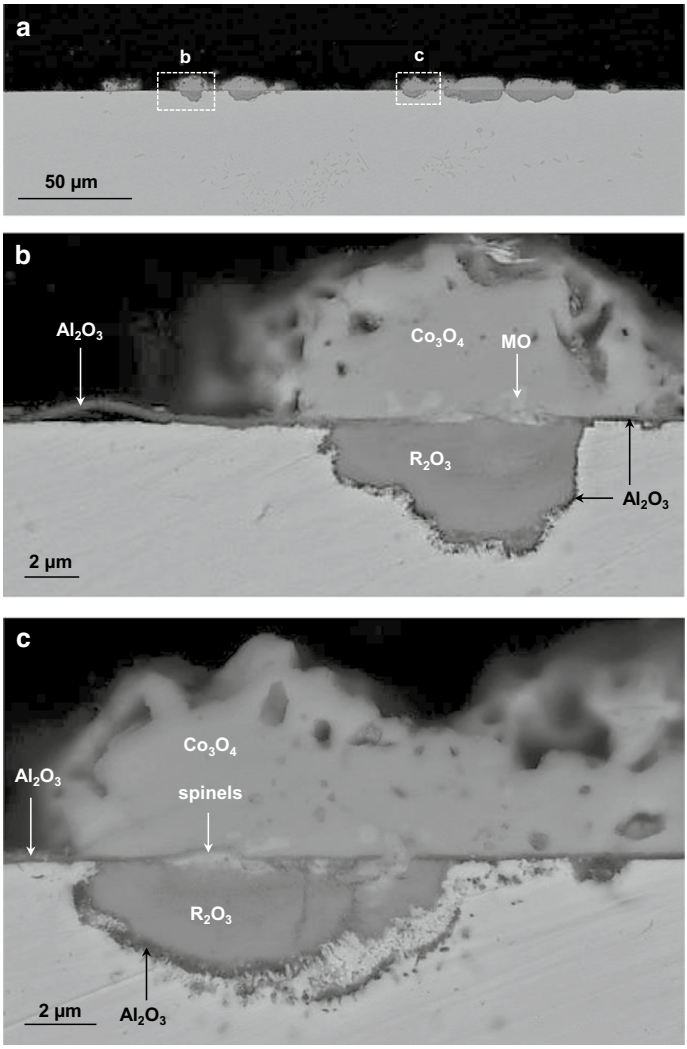


**Fig. 12** Micrographs (SEM/BEI) of a cross section of Co-20Ni-15Cr-5Al oxidized in 1 atm $O_2$ at 800 °C for 24 h: **a** General view; **b**, **c** Enlarged views of the selected areas of (**a**); **d** EDS maps of (**c**)

I scales). Alloys of group II, with larger contents of aluminum and chromium, form scales presenting a composition similar to those of produced by alloys of group I, except for a reduced relative thickness of the external CoO layer, which becomes similar to that of the inner layer: in both cases aluminum undergoes an internal oxidation (type II scales). The scales produced by alloys of group III (type III scales) involve an external oxidation of chromium coupled to an internal oxidation of aluminum, while the oxidation of cobalt is suppressed. Finally, alloys of group IV correspond to the exclusive growth of external alumina scales, while cobalt and chromium are no longer oxidized (type IV scales). For the present quaternary

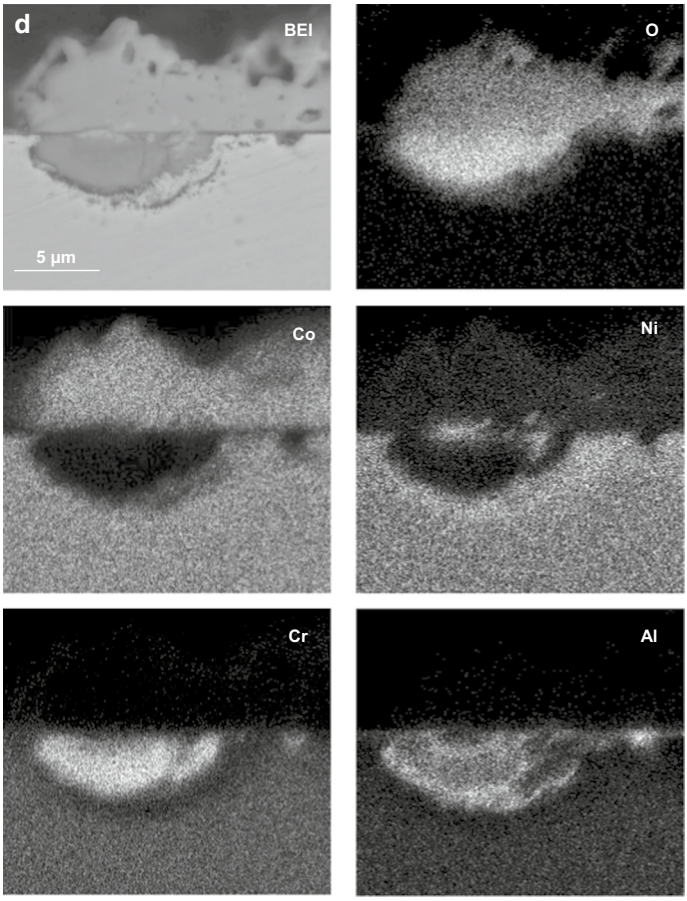


**Fig. 12** (continued)

Co-20Ni-base alloys containing chromium and aluminum the simple cobalt monoxide, CoO is replaced by solid solutions of CoO and NiO, MO, while spinels will generally contain appropriate combinations of divalent (Co,Ni) and trivalent (Cr,Al) metal ions. Furthermore, as a result of the temperature range selected, cobalt is also able to form the higher oxide $Co_3O_4$.

Despite its apparent generality, this classification does not yet give an exhaustive description of the actual structure of the scales produced by the oxidation of the present alloys. In fact, very often different oxidation mechanisms coexist simultaneously on the surface of the same sample, albeit with different relative abundance depending on the alloy composition and reaction temperature, so that in most cases the results for a single sample correspond to more than a single oxidation mode. Moreover, other types of structure not strictly considered in the previous list must also be taken into account. For example, thin external scales are frequently composed of an innermost layer of alumina surmounted by an external layer made of

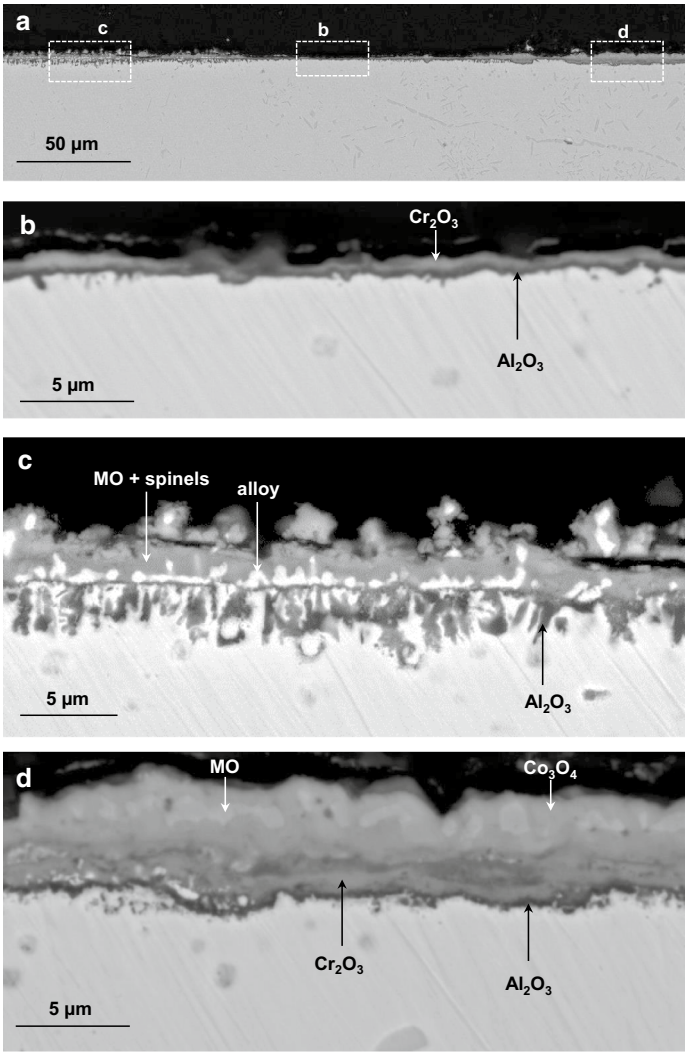


**Fig. 13** Micrographs (SEM/BEI) of a cross section of Co-20Ni-15Cr-5Al oxidized in 1 atm $O_2$ at 900 °C for 24 h: **a** General view; **b**, **c**, **d** Enlarged views of the selected areas of (**a**); **e** EDS maps of (**d**)

chromia or of spinels, but possibly containing also cobalt and nickel oxides, such as observed in the oxidation of Co-20Ni-15Cr-5Al at 900 °C: scales with this structure are still considered to belong to type IV. Moreover, in some cases, such as for the oxidation of Co-20Ni-8Cr-3Al or of Co-20Ni-8Cr-5Al at 900 °C, scales of type II are partly underlay by a thin alumina layer in contact with the alloy, not considered for type II scales: scales with this structure are still considered to belong to type II. Finally, the internal oxidation of aluminum beneath an external layer of chromia, expected for type III scales, may also occur beneath an external layer containing also

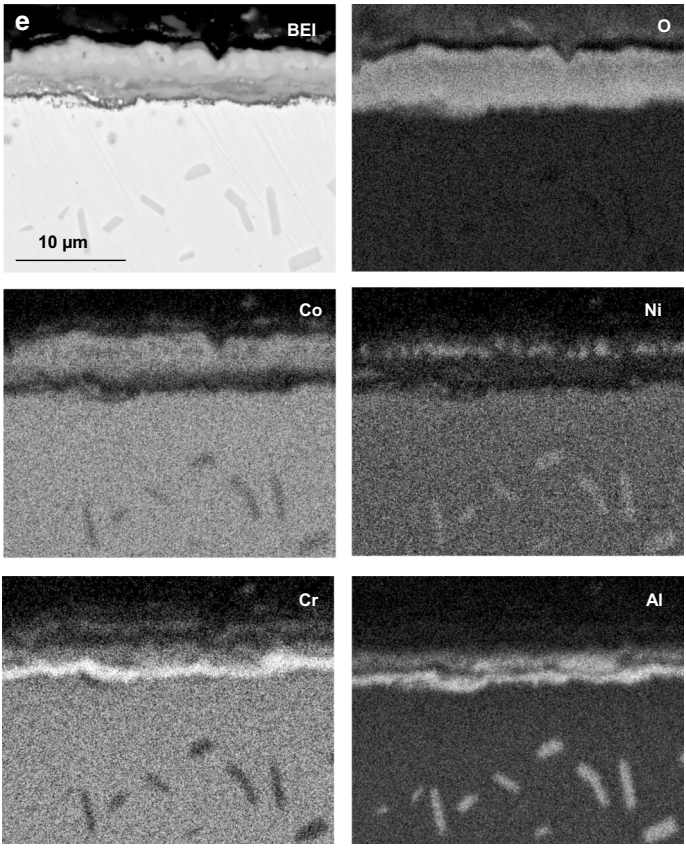


**Fig. 13** (continued)

**Table 2** Classification of the scales grown on the four Co-20Ni-xCr-yAl ($x = 8,15$ wt.%; $y = 3,5$ wt.%) alloys into the four scale types proposed by Wallwork and Hed [7] (*)

| T (°C) | 800 | 900 |
|---|---|---|
| Co-20Ni-8Cr-3Al | Type II + Type IV | Type II |
| Co-20Ni-8Cr-5Al | Type II + Type IV | Type II |
| Co-20Ni-15Cr-3Al | Type II (**) + Type IV | Type II + Type III |
| Co-20Ni-15Cr-5Al | Type II (**) + Type IV | Type III + Type IV |

*The assignment of two different groups for a given alloy at a constant temperature indicates the simultaneous presence of two different types of scale structure over different areas of the same sample

**With only few nodules of type II

spinels and possibly Co–Ni oxides, as observed for the oxidation of Co-20Ni-15Cr-5Al at 900 °C, a situation still considered to be of type III.

An approximate allocation of the scales observed after oxidation of the present four quaternary alloys at 800 °C and 900 °C to the four scale types recalled

above, taking into account the extensions proposed above, is given in Table 2. In particular, oxidation of the two alloys with 8 wt.% Cr produced scales of mixed types II and IV by oxidation at 800 °C, but mostly of type II by oxidation at 900 °C. Conversely, oxidation of the two alloys with 15 wt.% Cr and 3 or 5 wt.% Al produced mainly scales of type IV with type II nodules by oxidation at 800 °C, while by oxidation at 900 °C, Co-20Ni-15Cr-3Al formed scales of mixed types II and III and Co-20Ni-15Cr-5Al scales of mixed types III and IV. It is finally noted that the present results differ partly from the model proposed by Walkwork and Hed [7] because in some cases the outer layers of scales of type III are composed of spinels rather than chromia.

The reason for the presence of the higher cobalt oxide, $Co_3O_4$, in the external region of the scales grown on these four alloys is that the oxygen pressure adopted in the present tests is larger than that for the $CoO/Co_3O_4$ equilibrium at these two temperatures (equal to $4.26\times10^{-3}$ atm and 0.141 atm at 800 and 900 °C, respectively) [1]. In particular, $Co_3O_4$ formed isolated particles by oxidation at 900 °C rather than a continuous layer, as observed by oxidation at 800 °C, due to the smaller difference between the oxygen pressure in the gas phase and that for the equilibrium between the two oxides, which may have been further reduced due to the presence of some nickel dissolved in CoO, but not in $Co_3O_4$.

## Oxidation Kinetics

A general feature concerning the oxidation of these four alloys is their rather irregular kinetic behavior, as evidenced in particular by the changes with time of the slope of the parabolic plots observed frequently. As already observed in a previous paper regarding the oxidation of the same alloys at 1000 and 1100 °C [32], this aspect is connected with the presence of different types of scales growing simultaneously over different regions of the alloy surface and especially with the very likely change of their relative importance as the reaction proceeds. Effects of this kind have been observed experimentally and explained theoretically in a study of the time evolution of the nature of the scales produced by oxidation of some Ni-Cr-Al alloys able to form alumina scales by Nijdam et al. [13, 14]. These authors were able to identify four successive stages characterized by different kinetic behaviors corresponding to the growth of different types of scales during the same test before the final stable scale structure was established. In the present case the alloy with the smallest chromium and aluminum contents, Co-20Ni-8Cr-3Al, corroded much more rapidly than the other three alloys at both temperatures, with the exception of Co-20Ni-8Cr-5Al which at 800 °C corroded at approximately the same rate as the alloy with 8 wt.% Cr and 3 wt.% Al. These two alloys corroded significantly more slowly at 800 °C than at 900 °C mainly due a partial growth of type IV scales at 800 °C, absent at the higher temperature. The oxidation rates of Co-20Ni-15Cr-3Al and Co-20Ni-15Cr-5Al at 800 °C are slower than those of the alloys with same aluminum contents but containing only 8 wt.% Cr. The reason of this effect is that increasing the chromium content promotes the relative importance of scales of type IV, while at the same time that of scales of type II is significantly reduced. In summary, no exclusive

formation of an alumina scale has been observed, as already reported for the oxidation of the same alloys at 1000 and 1100 °C [32], even though significant amounts of alumina formed on the four alloys at 800 °C. Conversely, oxidation at 900 °C produced important amounts of alumina only for Co-20Ni-15Cr-5Al. In any case, an aluminum content up to 5 wt.% is still insufficient to form exclusive external alumina scales by oxidation of quaternary alloys of the composition examined in this work both at 800 and 900 °C even when combined with the presence of 15 wt.% chromium.

The comparison between the kinetics of oxidation of the present quaternary alloys at 800 °C and 900 °C with those of ternary alloys based on Co-20Ni and containing only aluminum or chromium as a third component at the same temperature, summarized by means of Figs. 4 and 5, respectively, leads to the following considerations. At 800 °C (Fig. 4) the mass gains of the quaternary alloys are considerably smaller than those of the corresponding ternary Co-20Ni-xCr and Co-20Ni-yAl alloys. Moreover, the increase of the aluminum content from 3 to 5 wt.% has a negligible effect on the oxidation resistance of the alloys containing either 8 or 15 wt.% chromium. Conversely, the increase of the chromium content from 8 to 15 wt.% has a clear positive effect on the oxidation resistance of the alloys containing either 3 or 5 wt.% aluminum. Thus, from a kinetic point of view, the effect of the addition of 3 wt.% or 5 wt.% aluminum is approximately the same for both ternary Co-20Ni-xCr alloys, while the addition of 15 wt.% chromium is much more effective than that of 8 wt.% chromium for both ternary Co-20Ni-yAl alloys. In any case, only the simultaneous presence of both protective elements has a strong positive effect on the kinetics of oxidation of these quaternary alloys. At this temperature, at variance with the quaternary alloys, all the ternary Co-20Ni-R alloys significantly more rapidly than the binary Co-20Ni alloy. A similar effect, already reported for binary alloys based on nickel or cobalt and containing chromium or aluminum, was attributed to an enhanced diffusion through the base MO oxide due to a doping effect produced by the presence of the trivalent ions $Cr^{3+}$ or $Al^{3+}$ in solution, which increases the concentration of metal vacancies of the base oxide, producing a faster diffusion of the base-metals ions through the scale [1, 34–39].

The situation observed at 900 °C (Fig. 5) is more complex. In fact, the mass gains of the quaternary alloys are again smaller than those of the ternary alloys with the same content of either chromium of aluminum, except for the case of Co-20Ni-15Cr-3Al which initially corrodes more slowly than the ternary alloy Co-20Ni-15Cr, but more rapidly than the same ternary alloy for sufficiently long times [33]. Moreover, at this temperature Co-20Ni-15Cr corrodes much more slowly also than the binary Co-20Ni alloy, at variance with the behavior of the other three ternary alloys [33]. Finally, an increase of the aluminum content from 3 to 5 wt.% improves the corrosion resistance for both the quaternary alloys containing 8 wt.% or 15 wt.% chromium. A similar effect is also produced by increasing the chromium content from 8 to 15 wt.% for both the quaternary alloys containing 3 wt.% or 5 wt.% aluminum. Thus, even at this temperature the best kinetic effect is obtained by the simultaneous addition of the two reactive alloy components, with the possible exception of Co-20Ni-15Cr-3Al which at long times corrodes faster than the ternary alloy Co-20Ni-15Cr.

### Effects of the Simultaneous Presence of Cobalt and Nickel

A final aspect of interest of the present results regards the effects of the simultaneous presence of cobalt and nickel on the oxidation behavior of the quaternary Co-20Ni-xCr-yAl alloys as compared with the results of the oxidation of ternary Co-Cr-Al and Ni-Cr-Al alloys of similar composition, with a particular attention to the critical chromium and aluminum contents needed to produce exclusive external alumina scales. For this, reference is made to the approximate oxide map of the pseudo-ternary M-Cr-Al system (where M is Ni + Co) established by Seraffon et al. [26] for the oxidation of a number of quaternary Co-Ni-Cr-Al alloys at 900 °C, shown in Fig. 14, where the data concerning the alloys studied in this paper at the same temperature have also been included. All the present alloys are located outside the region of stability of external alumina scales, or Region I, limited by the approximate boundary dashed line of Fig. 14, in agreement with the corresponding experimental results.

A further evidence to support to this conclusion is provided by the oxide maps for the oxidation at 900 °C of ternary Co-Cr-Al alloys and Ni-Cr-Al alloys, shown in Figs. 15 and 16, respectively, which contain also the composition of alloys with the same chromium and aluminum contents as the present quaternary alloys (denoted as equivalent ternary alloys). Due to the small number of experimental data, Fig. 15 contains only two points for ternary alloys [40] plus two points for binary Co-Al alloys [35], so that it is only possible to draw a very rough boundary line of Region I. Nonetheless, this map shows that both the chromium and aluminum contents of the equivalent ternary Co-Cr-Al alloys are much smaller than that of the only ternary alloy forming alumina scales. Furthermore, the larger aluminum contents of the two present Al-rich alloys (10.12 and 10.26 at.%) are much smaller than that of the first binary Co-Al alloy forming alumina scales (with about 20 at.%Al) and

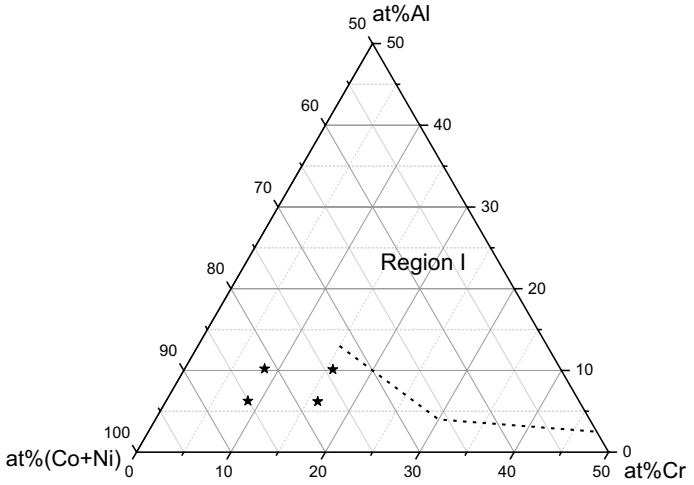


**Fig. 14** Simplified oxide map for quaternary Co-Ni-Cr-Al alloys exposed in 1 atm $O_2$ at 900 °C: the dashed line shows the boundary of the region of stability of alumina scales according to the results by Seraffon et al. [26]. The black stars correspond to the present quaternary Co-Ni-Cr-Al alloys

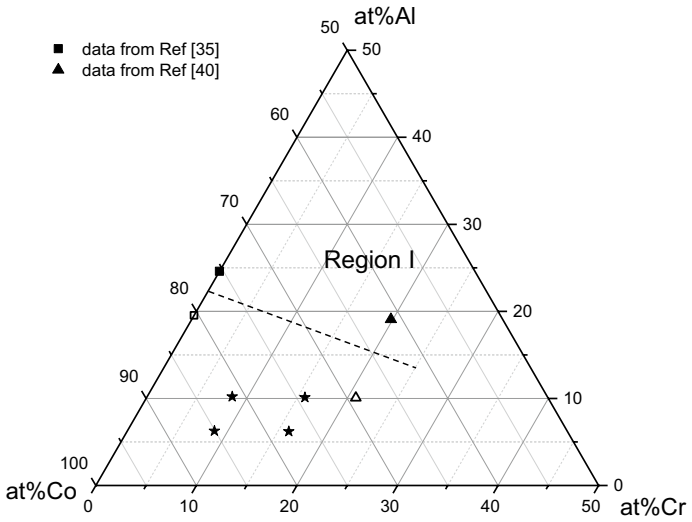


**Fig. 15** Simplified oxide map for ternary Co-Cr-Al alloys exposed in 1 atm $O_2$ at 900 °C: the dashed line shows an approximate boundary of the region of stability of alumina scales (Region I). The hollow symbols correspond to alloys forming external alumina scales; the black symbols correspond to alloys not able to form external alumina scales; the black stars correspond to ternary Co-Cr-Al alloys equivalent to the present quaternary alloys

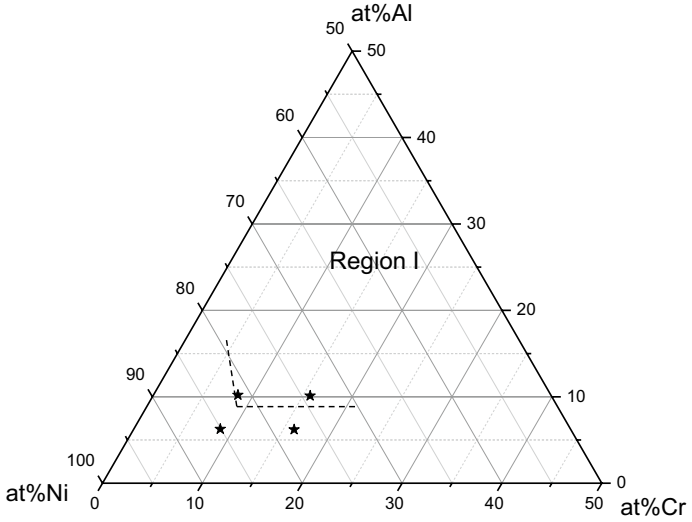


**Fig. 16** Simplified oxide map for ternary Ni-Cr-Al alloys exposed in 1 atm $O_2$ at 900 °C: the dashed line shows an approximate boundary of the region of stability of alumina scales (Region I) according to Seraffon et al. [26]. The black stars correspond to ternary Ni-Cr-Al alloys equivalent to the present quaternary alloys

approximately the same as that of the alloy not able to form alumina scales (with about 10 at.% Al). Conversely, the oxide map for ternary Ni-Cr-Al alloys (Fig. 16) at 900 °C taken from a paper by Seraffon et al. [26], based on a larger number of data (only the boundary line of region I is reported for simplicity), indicates that the two ternary Ni-Cr-Al alloys with 3 wt.% aluminum should not be able to form alumina scales, while the two alloys with 5 wt.% Al are close to the line indicating the boundary of Region I. In any case, in spite of the limited amount of data available, comparison between Figs. 15 and 16 suggests that the growth of external alumina scales is much more favorable for ternary M-Cr-Al alloys based on nickel than on similar alloys based on cobalt. Finally, a negative effect of a partial substitution of cobalt to nickel on the oxidation behavior of various complex alloys at high temperatures has been already reported by numerous previous studies [21, 23, 24, 29, 30].

## Conclusions

Four Co-20Ni-xCr-yAl ($x = 8,15$ wt.%; $y = 3,5$ wt.%) alloys were oxidized under 1 atm $O_2$ at 800 °C and 900 °C. At 800 °C external alumina scales formed only on a fraction of the surface of all alloys, more extended for the two alloys with 15 wt.% Cr. The remaining surface fraction was covered by thicker double-layered external scales of complex nature, mostly followed by an internal oxidation zone (IOZ) of aluminum. Conversely, oxidation at 900 °C the two alloys with 8 wt.% Cr produced duplex external scales plus an IOZ of aluminum. By oxidation at 900 °C Co-20Ni-15Cr-3Al formed a combination of thin chromia-rich scales overlying an IOZ of aluminum with thick scales having the usual complex composition. Finally, oxidation at 900 °C of Co-20Ni-15Cr-5Al produced alumina scales over about half of the alloy surface, while the remainder surface formed a complex external scale associated with an IOZ of aluminum. Altogether, except for the oxidation of Co-20Ni-15Cr-5Al at 900 °C, the tendency to form external alumina scales is stronger at 800 °C that at 900 °C. However, under the present testing conditions an aluminum content of 5 wt.% is still insufficient to form exclusive external alumina scales on alloys containing up to 15 wt.% Cr.

The partial replacement of cobalt by nickel has a beneficial effect on the ability of the quaternary Co-20Ni-xCr-yAl alloys to form protective external alumina scales as compared with ternary Ni-Cr-Al alloys with similar chromium and aluminum contents. Finally, the simultaneous presence of chromium or aluminum is beneficial to reduce the oxidation rate of quaternary Co-20Ni-xCr-yAl alloys with respect to ternary Co-20Ni-Cr and Co-20Ni-Al alloys with the same chromium or aluminum contents.

**Acknowledgements** This work was supported by the NSFC Projects (No.52171066 and No.51771034), Graduate Scientific Research Innovation Project of Hunan Province (No. CX20200871) and Graduate Scientific Research Innovation Project of CSUST (No. CX2020SS66).

**Data Availability** The raw/processed data required to reproduce these findings cannot be shared at this time as the data also forms part of an ongoing study.

## References


1. D.J. Young, *High Temperature Oxidation and Corrosion of Metals*, Second Edition, (Elsevier Corrosion Series, New York, 2016).
2. G.R. Lai, *High-Temperature Corrosion and Materials Applications*, (ASM International, 2007).
3. R. Prescott and M. J. Graham, *Oxidation of Metals* **38**, 233 (1992).
4. P. Y. Hou, *Journal of the American Ceramic Society* **86**, 660 (2003).
5. F. H. Stott, G. C. Wood, and J. Stringer, *Oxidation of Metals* **44**, 113 (1995).
6. N. S. Jacobson, M. A. Kuczmarski, and B. A. Kowalski, *Oxidation of Metals* **93**, 247 (2020).
7. G. R. Wallwork and A. Z. Hed, *Oxidation of Metals* **3**, 213 (1971).
8. G. R. Wallwork and A. Z. Hed, *Oxidation of Metals* **3**, 243 (1971).
9. H. Stott, G. C. Wood, and M. G. Hobby, *Oxidation of Metals* **3**, 103 (1971).
10. G. N. Irving, J. Stringer, and D. P. Whittle, *Corrosion* **33**, 56 (1977).
11. L. Hu, D. B. Hovis, and A. H. Heuer, *Oxidation of Metals* **73**, 275 (2010).
12. A. Ul-Hamid, *Corrosion Science* **46**, 27 (2004).
13. T. J. Nijdam, L. P. H. Jeurgens, and W. G. Sloof, *Materials at High Temperatures* **20**, 311 (2003).
14. T. J. Nijdam, L. P. H. Jeurgens, and W. G. Sloof, *Acta Materialia* **53**, 1643 (2005).
15. I. A. Kvernes and P. Kofstad, *Metallurgical Transactions* **3**, 1511 (1972).
16. Y. Niu, X. J. Zhang, Y. Wu, and F. Gesmundo, *Corrosion Science* **48**, 4020 (2006).
17. X. J. Zhang, S. Y. Wang, F. Gesmundo, and Y. Niu, *Oxidation of Metals* **65**, 151 (2006).
18. S. R. LeVine, *Metallurgical Transactions A* **99**, 1237 (1978).
19. M. Weiser, Y. M. Eggeler, E. Spiecker, and S. Virtanen, *Corrosion Science* **135**, 78 (2018).
20. L. Klein, A. Bauer, S. Neumeier, M. Göken, and S. Virtanen, *Corrosion Science* **53**, 2027 (2011).
21. B. Gao, L. Wang, Y. Liu, X. Song, S. Y. Yang, and A. Chiba, *Corrosion Science* **157**, 109 (2019).
22. B. H. Yu, Y. P. Li, Y. Nie, and H. Mei, *Journal of Alloys and Compounds* **765**, 1148 (2018).
23. F. B. Ismail, V. A. Vorontsov, T. C. Lindley, M. C. Hardy, D. Dye, and B. A. Shollock, *Corrosion Science* **116**, 44 (2017).
24. M. Weiser, M. G. Galetz, R. J. Chater, and S. Virtanen, *Journal of the Electrochemical Society* **167**, 021504 (2020).
25. M. Seraffon, N. J. Simms, J. Summer, and J. R. Nicholls, *Surface and Coatings Technology* **206**, 1529 (2011).
26. M. Seraffon, N. J. Simms, J. Summer, and J. R. Nicholls, *Oxidation of Metals* **81**, 203 (2014).
27. H. Lan, P. Y. Hou, Z. G. Yang, Y. D. Zhang, and C. Zhang, *Oxidation of Metals* **75**, 77 (2011).
28. L. Yang, Y. Zheng and Z.G. Yang, *TMS 2020 149th Annual Meeting & Exhibition Supplemental Proceedings.* 763 (2020).
29. M. Weiser, M. C. Galetz, H. Eberard-Zschau, C. H. Zenk, S. Neumeier, M. Goken, and S. Virtanen, *Corrosion Science* **156**, 84 (2019).
30. C. H. Zenk, S. Neumeier, N. M. Engl, S. G. Fries, O. Dolotko, M. Weiser, S. Virtanen, and M. Goken, *Scripta materialia* **112**, 83 (2016).
31. B. D. Bastow, D. P. Whittle, and G. C. Wood, *Corrosion Science* **16**, 57 (1976).
32. Y. J. Ren, T. Dai, X. H. Guo, J. Shen, Y. L. Lv, J. Chen, and Y. Niu, *Corrosion Science* **191**, 109719 (2021).
33. Y. L. Lv, Y. J. Ren, W. Wang, L. B. Zhou, J. Chen, J. Huang, M. S. Tao, and Y. Niu, *Corrosion Science* **199**, 110140 (2022).
34. F. S. Pettit, *Transactions of the Metallurgical Society of AIME* **239**, 1296 (1967).
35. G. N. Irving, J. Stringer, and D. P. Whittle, *Oxidation of Metals* **9**, 427 (1975).
36. C. S. Giggins and F. S. Pettit, *Journal of the Electrochemical Society* **118**, 1782 (1971).
37. G. C. Wood, F. H. Stott, and J. E. Forrest, *Materials and Corrosion* **28**, 395 (1977).
38. F. H. Stott, I. G. Wright, T. Hodgkiess, and G. C. Wood, *Oxidation of Metals* **11**, 141 (1977).
39. I. G. Wright and G. C. Wood, *Oxidation of Metals* **11**, 163 (1977).
40. H. Yu, S. Ukai, S. Hayaschic, and N. Oono, *Corrosion Science* **118**, 49 (2017).